Nanotubular structures via templateless electropolymerization using thieno[3,4-b]thiophene monomers with various substituents and polar linkers

Salif Sow, Abdoulaye Dramé, El Hadji Yade Thiam, François Orange, Aboubacary Sene, Samba Yandé Dieng, Frédéric Guittard, Thierry Darmanin

Nanotubular structures via templateless electropolymerization using thieno[3,4-*b*]thiophene monomers with various substituents and polar linkers

Salif Sow[a], Abdoulaye Dramé[a], El hadji Yade Thiam[a], François Orange[b], Aboubacary Sene[a], Samba Yandé Dieng[a], Frédéric Guittard[c,d] and Thierry Darmanin[c,*]

[a]*Université Cheikh Anta Diop, Faculté des Sciences et Techniques, Département de Chimie, B.P. 5005 Dakar, Sénégal.*

[b]*Université Côte d'Azur, CCMA, 06100, Nice, France.*

[c]*Université Côte d'Azur, NICE Lab, IMREDD, 61-63 Av. Simon Veil, 06200 Nice, France.*

Corresponding author: thierry.darmanin@unice.fr

[d]*University California Riverside, Department of Bioengineering, Riverside, CA, USA*

Abstract

In this work, we investigate original thieno[3,4-*b*]thiophene monomers with polar carbamate linkers and various substituents and demonstrate the ability to prepare nanoporous structures via templateless, surfactant-free electropolymerization in organic solvent (dichloromethane). Including a significant amount of water in the electropolymerization solvent often leads to the formation of nanoporous structures with tunable size and surface hydrophobicity. Here, hollow spheres or nanorings are observed with thieno[3,4-*b*]thiophene monomers with alkyl chains. By contrast, using thieno[3,4-*b*]thiophene monomers with aromatic groups nanotubular structures are observed. For most of them, an increase in the surface hydrophobicity and water adhesion is observed. These innovative surfaces and the ease at which they can be fabricated are extremely interesting for applications in water harvesting systems, separations membranes, opto-electronic devices as well as for sensors.

Keywords: Nanotubes, Nanostructures, Electropolymerization, Conducting polymers, Wettability.

Introduction

Nanoporous interfaces such as nanotube arrays have gathered significant interest over recent years due to their large surface area and their potential applications in sensors, optical, photocatalysis, magnetism, energy storage and electronic devices, as well as for the manipulation of surface wetting properties [1–15]. Similar to the adhesive properties of gecko pads, both surface hydrophobicity and water adhesion of nanoporous interfaces are highly dependent on the geometry of nanotube arrays (e.g., diameter, height, pore size and spacing between nanotube features) [16–23]. For developing these well-ordered surfaces, researchers often rely on hard or rigid templates, such as anodized aluminum/titanium membranes, to direct the formation of tubular and porous features [24–26]. However, templated processes are lengthy and challenging to implement, especially on a large scale and a new template is required for any modification to the surface geometry within the nanotube array [27,28].

To avoid the need for templates, templateless electropolymerization is an alternative that enables rapid preparation of highly ordered, nanotube structures. As an example, electropolymerization of pyrrole in aqueous solutions has been studied by many different research groups to create this class of structures [29–39]. When polymerized in water (H_2O), the formation of porous structures from pyrrole is attributed to the *in situ* release of gas bubbles (H_2 and/or O_2) from H_2O directly during electropolymerization. While the exploitation of this gas release is a relatively straightforward process, a surfactant is necessary in order to stabilize the gas bubbles and form the porous structures. Moreover, most pyrrole-based monomers are not soluble in water and therefore electropolymerization in water often requires a very high monomer concentration. Recent studies have identified approaches that eliminate this need for surfactant, and thus permit the formation of tubular features via electropolymerization in organic solvent (e.g., CH_2Cl_2) [40–45] containing trace H_2O. With this approach, vertically aligned nanotubes with high water adhesion have been developed using rigid monomers such as 3,4-phenylenedioxythiophene (PheDOT), naphthalenedioxythiophene (NaphDOT) and thienothiophene derivatives. In these examples, the monomer rigidity is a key parameter to stabilize gas bubbles during electropolymerization. Due to their high rigidity and exceptional opto-electronic properties, thieno[3,4-*b*]thiophene monomers and associated analogues have proven to be excellent candidates to obtain nanoporous structures such as nanotubes *via* templateless electropolymerization [43–47]. Using thieno[3,4-*b*]thiophene derivatives, it has been demonstrated that with a significant

amount of water in dichloromethane (dichloromethane saturated with water vs. commercial dichloromethane) the surface morphology is drastically altered. In this study, knowing that water plays a crucial role in templateless electropolymerization, we demonstrate that it is possible to control the surface structures by judicious selection of polar linkers able to form hydrogen bonds incorporated onto thieno[3,4-*b*]thiophene derivatives [48]. The studied monomers are represented in Scheme 1. During electropolymerization, we employed two different solvents: dichloromethane (CH_2Cl_2) and dichloromethane saturated with water ($CH_2Cl_2 + H_2O$).

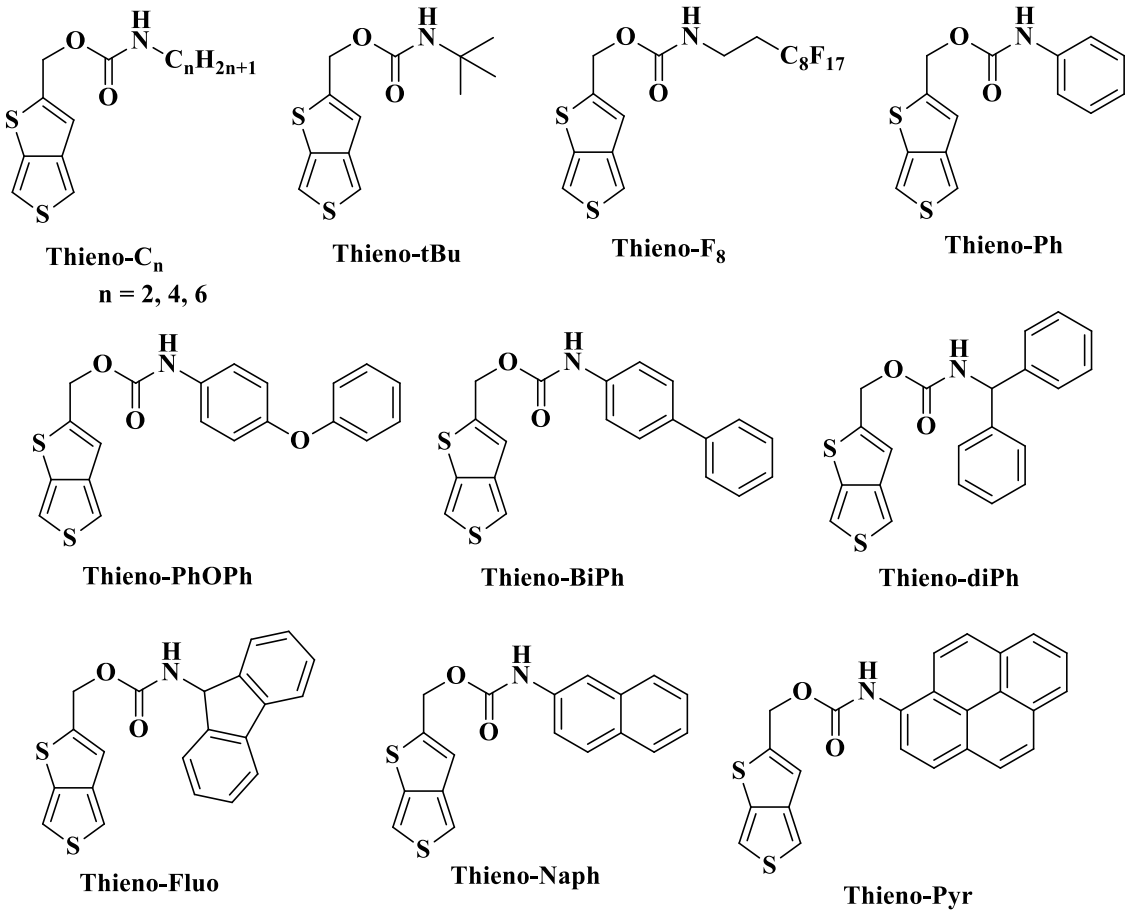

Scheme 1. Monomers investigated in this work.

2. Experimental Section

2.1. Monomer synthesis

The synthetic route employed to develop the monomers of interest is represented in Scheme 2. First, thieno[3,4-*b*]thiophen-2-ylmethanol (Thieno-OH) was synthesized in three steps from 3,4-dibromothiophene, following a procedure already reported in the literature [49–51]. After this procedure, 1 eq. (200 mg) Thieno-OH and 1.2 eq. of the selected isocyanate were dissolved in 20 ml of anhydrous dichloromethane. Approximately 10 drops (1.5 ml) of triethylamine were added as the catalyst progressed. The mixture was stirred at room temperature for 24 h. The products were purified by column chromatography on silica gel (ether / cyclohexane of the same volume as eluent).

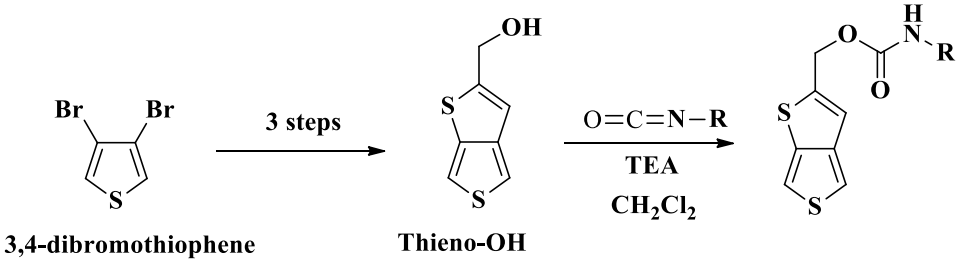

Scheme 2. Chemical way to the monomers.

Thieno-C2: thieno[3,4-*b*]thiophen-2-ylmethyl ethylcarbamate. Yield 30%; White solid; δ_H(400 MHz, $CDCl_3$): 7.34 (d, 1H, J = 2.7 Hz), 7.26 (d, 1H, J=2.7MHz), 6.90 (s, 1H), 5.17 (s, 2H), 4.78 (1H, s), 3.25 (m, 2H), 1.14 (t, 3H, J=7.3MHz); δ_C(400MHz, $CDCl_3$): 154.74, 146.46, 144.65, 136.36, 115.74, 111.50, 109.75, 61.32, 34.97, 14.17; MS (70 eV): m/z 241 (M^+, 18), 170 ($C_7H_6OS_2^+$, 100).

Thieno-C4: thieno[3,4-*b*]thiophen-2-ylmethyl butylcarbamate. Yield 60%; White solid; δ_H(400 MHz, $CDCl_3$): 7.34 (d, J = 2.7 Hz, 1H), 7.26 (d, 1H, J=2.7MHz), 6.90 (s, 1H), 5.17 (s, 2H), 4.77 (s, 1H), 3,21 (m, 2H), 1,45 (m, 4H), 0,90 (t, 3H, J = 7.2 Hz); δ_C(400MHz, $CDCl_3$) : 155.86, 146.46, 145.66, 139.12, 116.74, 112.49, 110.74, 62.34, 31.95, 30.29, 19.84, 13.68; MS (70 eV): m/z 269 (M^+, 13), 170 ($C_7H_6OS_2^+$, 100).

Thieno-C6: thieno[3,4-*b*]thiophen-2-ylmethyl hexylcarbamate. Yield 57%; White solid; δ_H(400 MHz, $CDCl_3$) : 7.34 (d, J = 2.7 Hz, 1H), 7.26 (d, 1H, J=2.7MHz), 6.90 (s, 1H), 5.17 (s, 2H), 4.77 (s, 1H), 3,17 (m, 2H), 1,45 (m, 2H), 1,28 (m, 6H), 0,90 (3H, t, J = 6.5 Hz); δ_C(400MHz, $CDCl_3$) : 155.86, 146.47, 145.66, 139.12, 116.74, 112.49, 110.74, 62.35, 41.17, 31.41, 29.85, 22.52, 13.97 ; MS (70 eV): m/z 297 (M^+, 10), 170 ($C_7H_6OS_2^+$, 100).

Thieno-tBu: thieno[3,4-*b*]thiophen-2-ylmethyl *tert*-butylcarbamate. Yield 51%; White solid; δ_H(400 MHz, $CDCl_3$) : 7.34 (d, J = 2.7 Hz, 1H), 7.26 (d, 1H, J=2.7MHz), 6.90 (s, 1H), 5.17

(2H, s), 4.78 (1H, s), 1.36 (m, 9H); δ_C(400MHz, $CDCl_3$) : 155.86, 146.46, 145.66, 139.12, 116.74, 112.49, 110.74, 62.34, 28.88.95, 26.89; MS (70 eV): m/z 269 (M^+, 10), 170 ($C_7H_6OS_2^+$, 100).

Thieno-F$_8$: thieno[3,4-*b*]thiophen-2-ylmethyl (3,3,4,4,5,5,6,6,7,7,8,8,9,9,10,10,10-heptadecafluorodecyl)carbamate. Yield 48%; White solid; δ_H(400 MHz, $CDCl_3$): 7.34 (d, J = 2.7 Hz, 1H), 7.26 (d, 1H, J=2.7MHz), 6.90 (s, 1H), 5.17 (2H, s), 4.77 (1H, s), 3,08 (t, 2H, J=6.2MHZ), 2.13 (t, 2H, J=6.3MHz); δ_C(400MHz, CDCl3) : 155.86, 146.47, 145.66, 139.12, 129.03, 121.52, 120.70, 116.74, 115.86, 115.73, 115.26, 112.67, 112.42, 111.14, 110.74, 62.35, 31.27, 29.36; MS (70 eV): m/z (M+, 100), 659 ($C_7H_5OS_2^+$, 13), 170 ($C_7H_6OS_2^+$, 100).

Thieno-Ph: thieno[3,4-*b*]thiophen-2-ylmethyl phenylcarbamate. Yield 79%; White solid; δ_H(400 MHz, $CDCl_3$): 7.42 (m, 4H), 7.36 (m, 1H), 7.32 (d, 1H, J=2.7MHz), 7.26 (d, 1H, J=2.7MHz), 7.24 (s, 1H), 7.01 (s, 1H), 5.27 (s, 2H); δ_C (400MHz, $CDCl_3$): 155.86, 145.47, 141.66, 135.38, 132.16, 131.68, 131.32, 130.78, 130.51, 128.82, 124.74, 112.49, 62.35 ; MS (70 eV): m/z 289 (M^+, 7), 170 ($C_7H_6OS_2^+$, 16).

Thieno-PhOPh: thieno[3,4-*b*]thiophen-2-ylmethyl (4-phenoxyphenyl)carbamate. Yield 85%; White solid; δ_H(400 MHz, $CDCl_3$) : 7.69 (m, 2H), 7.33 (m, 2H), 7.31 (d, 1H, J=2.7MHz), 7.28 (d, 1H, J=2.3MHz), 7.08 (m, 2H), 7.09 (m, 2H), 6.99 (s, 1H), 6.78 (s, 1H), 5.27 (s, 2H) ; δ_C(400MHz, $CDCl_3$): 162.07, 156.91, 155.84, 142.76, 134.02, 133.51, 131.57, 130.95, 130.31, 132.52, 129.33, 124.35, 123.73, 122.69, 122.54, 64.25.

Thieno-BiPh: thieno[3,4-*b*]thiophen-2-ylmethyl [1,1'-biphenyl]-4-ylcarbamate. Yield 22%; White solid; δ_H(400 MHz, $CDCl_3$): 7.59 (m, 2H), 7.53 (m, 2H), 7.50 (m, 2H), 7.36 (m, 2H), 7.29 (d, 1H, J=2.7MHz), 7.25 (d, 1H, J=2.4MHz), 7.24 (m, 1H), 7.22 (s, 1H), 6.89 (s, 1H), 5.27 (s, 2H; δ_C(400MHz, $CDCl_3$): 155.36, 144.81, 143.56, 140.83, 138.12, 137.16, 135.37, 133.95, 133.71, 132.52, 131.63, 131.35, 128.13, 124.69, 62.35.

Thieno-diPh: thieno[3,4-*b*]thiophen-2-ylmethyl benzhydrylcarbamate. Yield 50%; White Solid; δ_H(400 MHz, $CDCl_3$): 7.36 (d, 1H, J=2.7MHz), 7.32 (d, 1H, J=2.3MHz), 7.26 (m, 2H), 7.27 (m, 4H), 7.17 (m, 4H), 6.91 (s, 1H), 6.26 (d, 1H, J=2.6MHz), 5.27 (s, 2H); δ_C(400MHz, $CDCl_3$): 156.36, 146.84, 142.66, 137.38, 135.36, 132.48, 132.32, 131.61, 131.28, 129.30, 121.74, 68.74, 62.36; MS (70 eV): m/z 379 (M^+, 15), 170 ($C_7H_6OS_2^+$, 100).

Thieno-Fluo: thieno[3,4-*b*]thiophen-2-ylmethyl 9*H*-fluoren-9-ylcarbamate. Yield 73%; White solid; δ_H(400 MHz, $CDCl_3$): 7.94 (m, 2H), 7.6 (m, 2H), 7.48 (m, 1H), 7.39 (m, 2H), 7.31 (d, 1H, J=2.6MHz), 7.28 (d, 1H, J=2.3MHz), 7.07 (s, 1H), 6.94 (s, 1H), 6.11 (d, 1H, J=2.5MHz),

5.27 (s, 2H); δ_C(400MHz, $CDCl_3$): 159.18, 145.92, 145.03, 143.83, 133.89, 133.47, 133.24, 131.81, 131.52, 130.68, 13.30, 129.35, 123.74, 63.56, 57.93.

Thieno-Naph: thieno[3,4-*b*]thiophen-2-ylmethyl naphthalen-2-ylcarbamate. Yield 43%; White solid; δ_H(400 MHz, CDCl3) : 7.95 (m, 1H), 7.80 (m, 1H), 7.76 (m, 1H), 7.46 (m, 1H), 7.34 (m, 1H), 7.33 (m, 1H), 7.23 (m, 1H), 7.22 (d, 1H, J=2.7MHz), 7.07 (d, 1H, J=2.7MHz), 6.99 (s, 1H), 6.88 (s, 1H), 5.27 (s, 2H); δ_C(400MHz, $CDCl_3$): 155.36, 144.82, 141.56, 139.78, 133.94, 132.84, 132.59, 132.55, 131.64, 131.38, 131.33, 130.65, 130.37, 127.42, 125.74, 125.12, 114.45, 62.35.

Thieno-Pyr: thieno[3,4-*b*]thiophen-2-ylmethyl pyren-1-ylcarbamate. Yield 93%; White solid; δ_H(400 MHz, $CDCl_3$): 8.10 (m, 9H), 7.31 (d, 1H, J=2.7MHz), 7.28 (d, 1H, J=2.7MHz), 6.88 (s, 1H), 6.81 (s, 1H), 5. 29 (s, 2H); δ_C(400MHz, CDCl3): 168.23, 145.74, 143.87, 137.45, 130.24, 129.97, 129.67, 128.62, 127.29, 126.83, 126.58, 126.32, 126.04, 125.61, 125.22, 124.90, 124.75, 124.13, 123.86, 122.15, 116.21, 111.67 109.82, 64.25.

2.2. Templateless electropoymerization

Electropolymerizations were performed using an Autolab potentiostat (Metrohm) equipped with a three-electrode system: a gold plate (2 cm^2) as the working electrode, a carbon-rod as the counter electrode and a saturated calomel electrode (SCE) as the reference electrode. The electrochemical solution was composed of 0.1 M of tetrabutylammonium perchlorate (Bu_4NClO_4) as the electrolyte and 0.01 M of the monomer of interest. In order to better evaluate the influence of H_2O content, two different solvents were employed: neat dichloromethane (CH_2Cl_2), and dichloromethane saturated with water (CH_2Cl_2 + H_2O). The latter was prepared by simply mixing CH_2Cl_2 with a high amount of deionized H_2O. Any additional H_2O remaining after mixing was removed by extraction.

For each synthesized monomer, the oxidation potential (E^{ox}) was first determined and the depositions were performed under potentiodynamic conditions via cyclic voltammetry at a scan rate of 20 mV s^{-1}. The total number of scans was varied (1, 3 and 5) in order to characterize polymer growth. After the appropriate number of scans, the substrates were washed three time in dichloromethane to remove any unreacted monomer or residual electrolyte.

2.3. Surface characterization

Surfaces structures were observed via scanning electron microscopy (SEM) using a 6700F microscope (JEOL). Surface wettability was characterized by goniometry using a DSA30 goniometer (Bruker) and the "Drop Shape Analysis System" software. Each data point presented reflects a mean of five measurements (n = 5). Water droplets (2 µL) were deposited onto surfaces and the apparent contact angles (θ_w) were determined at the triple point. The dynamic contact angles were obtained by the tilted droplet method using 6 µL water droplets. The maximum angle achieved before observation of droplet roll-off was measured and deemed the sliding angle (α). If no droplet roll-off was observed after an inclination of 90º, the water adhesion was considered extremely strong and the surface was then deemed sticky. For EDX analyses, samples were analyzed with a Tescan Vega 3 XMU scanning electron microscope (TESCAN FRANCE, Fuveau, France) equipped with an X-MaxN 50 EDX detector (Oxford Instruments, Abingdon, U.K.). Samples were carbon-coated prior to analyses (à modifier si tu mets les analyses des échantillons métallisés au Platine). All analyses were performed under identical conditions: an acceleration voltage of 10 kV, a 10 mm working distance and a 2000× magnification. EDX spectra were processed with the Aztec software (version 3.1, Oxford Instruments).

3. Results and Discussion

3.1. Electropolymerization

Templateless electropolymerization was performed in two different solvents in order to better understand the influence of H_2O content on the release of O_2/H_2 bubbles and the resulting surface structures. Cyclic voltammetry was first chosen as the electropolymerization method since it enables the release of a high amount of the two gas bubbles from H_2O if the potential range is sufficiently large (here from -1 V to E^{ox} vs SCE). More precisely, O_2 gas bubbles can be released during the forward scans (anodic) and H_2 during the back scans (cathodic). For the monomers synthesized in this study, the oxidation potentials (E^{ox}) were determined to be ≈ 1.70-1.80 V, depending on the structure. Therefore, electrodepositions were performed from -1 V to E^{ox} at a scan rate of 20 mV s^{-1} while the number of scans was varied (1, 3, or 5 scans) in order to observe the polymer growth.

Representative cyclic voltammograms for select monomers (Thieno-C_2, Thieno-C_4, Thieno-*t*Bu, and Thieno-Pyr) are presented in Figure 1. From these voltammograms, it is evident that the intensity of the polymer oxidation/reduction peaks is highest for Thieno-C_2, Thieno-*t*Bu,

and Thieno-Pyr, while the lowest intensity is observed for Thieno-Naph. This is likely due to the steric effects associated with the bulky side groups, which prevents tight packing of the neighboring polymer chains for Thieno-Naph. As a result, the thickness of polymer deposited after cyclic voltammetry is largest for polymers that have smaller side groups. In these cyclic voltammograms, it is also possible to observe peaks indicating the formation of O_2 bubbles from H_2O during forward scans (anodic scans) at roughly 1.5–2.0 V *vs.* SCE (**$2H_2O \rightarrow O_2$ *(bubbles)* + $4H^+$ + $4e^-$**), and the formation of H_2 bubbles from H_2O during back scans (cathodic scans) at roughly –0.5 V *vs.* SCE (**$2H_2O + 2e^- \rightarrow H_2$ *(bubbles)* + $2OH^-$**). Unfortunately, with these monomers, the peak for the formation of O_2 is more difficult to detect since E^{ox} occurs at roughly the same potentials (**nMonomer → Polymer + $2ne^-$ + $2nH^+$**), and thus cannot be isolated in this study. However, the peak of the formation of H_2 bubbles is clearly present in cyclic voltammograms for which the polymer oxidation/reduction peaks are not very intense such as with Thieno-Naph.

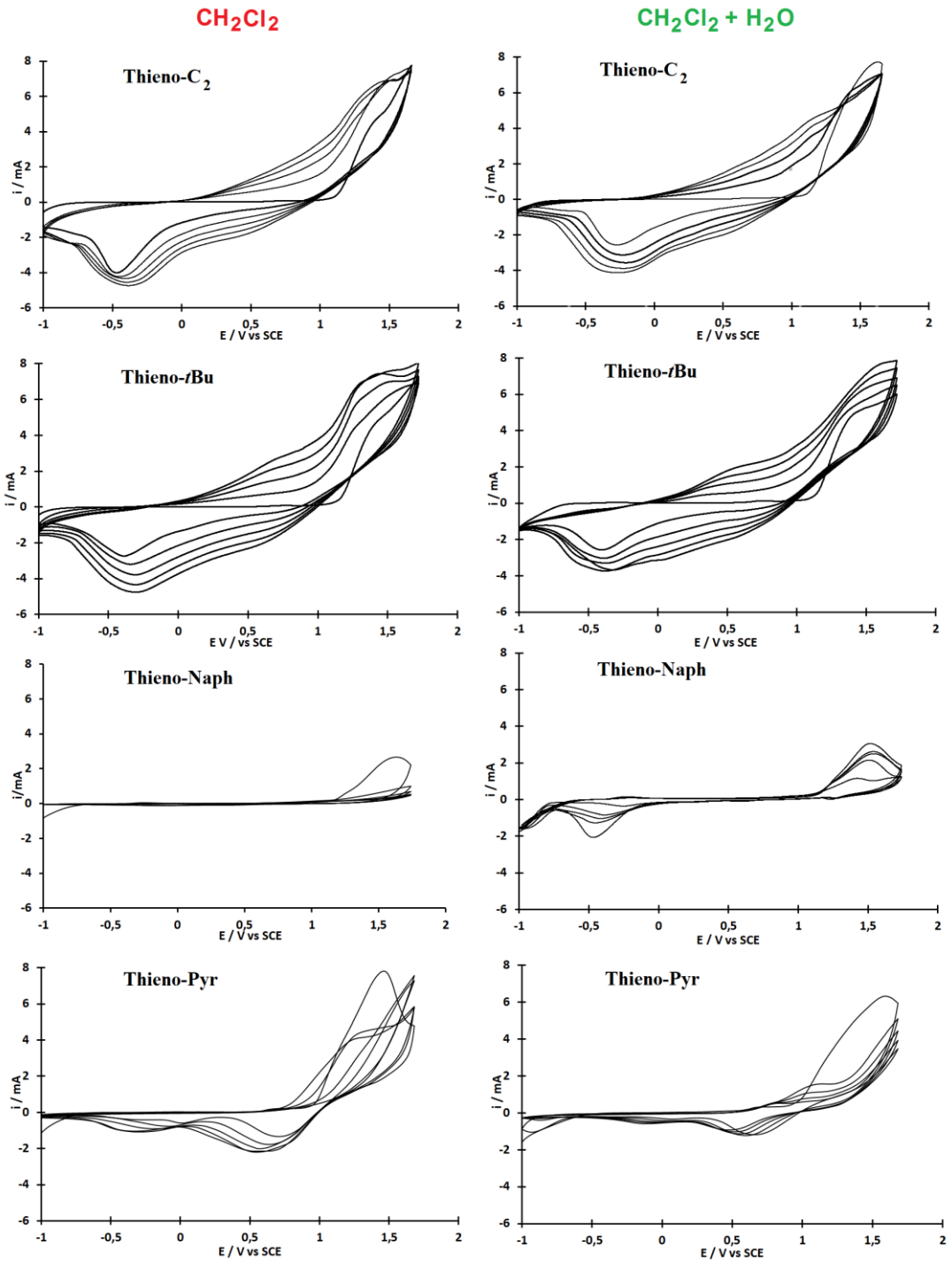

Figure 1. Cyclic voltammograms (5 scans) of select monomers (Thieno-C_2, Thieno-*t*Bu, Thieno-NaPh and Thieno-Py) in CH_2Cl_2 (left hand column) and CH_2Cl_2 + H_2O (right column) with Bu_4NClO_4 as electrolyte. Scan rate: 20 mV s^{-1}.

To better estimate the influence of H_2O, cyclic voltammograms were performed in CH_2Cl_2 or CH_2Cl_2 + H_2O without monomer (Figure 2). A significant peak at ≈ -0.5 V *vs* SCE is present during the back scan in CH_2Cl_2 + H_2O, confirming the reaction **2 H_2O + 2 e^- → H_2 (bubbles) + 2 OH^-**. This peak starts at ≈ -0.0 V and ends at ≈ -0.85 V. For the reaction **2 H_2O → O_2**

(bubbles) + 4 H^+ + 4 e^-, a peak is present during the forward scan but starts at ≈ 2.0 V *vs* SCE. Hence, in the potential range employed during the polymerizations here, the formation of H_2 bubbles is expected to have a more significant impact.

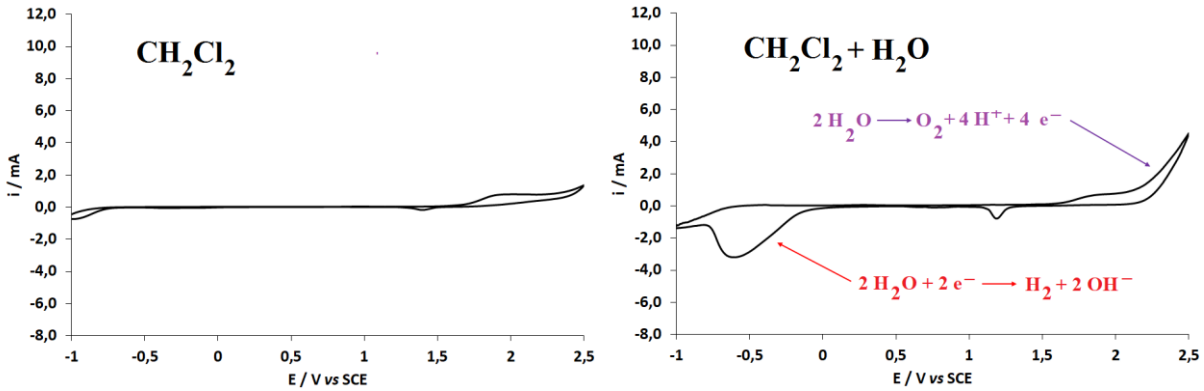

Figure 2. Cyclic voltammograms of CH_2Cl_2 or CH_2Cl_2 + H_2O with Bu_4NClO_4 (0.1 M); scan rate: 20 mV s^{-1}.

3.2. Surface properties

3.2.1. Surface morphology and wettability

Surfaces formed via electropolymerization were characterized by SEM and goniometry. H_2O content has a significant impact, and as expected the surfaces obtained in CH_2Cl_2 + H_2O are often more porous. Using monomers with alkyl chains, Thieno-C_n, the surfaces polymerized in CH_2Cl_2 are rough with some nanorings with a platelet shape present (Figure 3). However, a huge number of hollow spheres are clearly observed with some of the monomers polymerized in CH_2Cl_2 + H_2O. These spherical structures are obtained with monomers bearing short alkyl chains (Thieno-C_2 and Thieno-C_4). This indicates that the polymer rigidity is a key parameter in the formation of porous structures, and thus long alkyl chains are too flexible and do not form the porous structures. This reasoning can also justify why H_2O content does not impact the morphology of surfaces formed from monomers bearing very flexible hyperbranched alkyl chains (Thieno-*t*Bu).

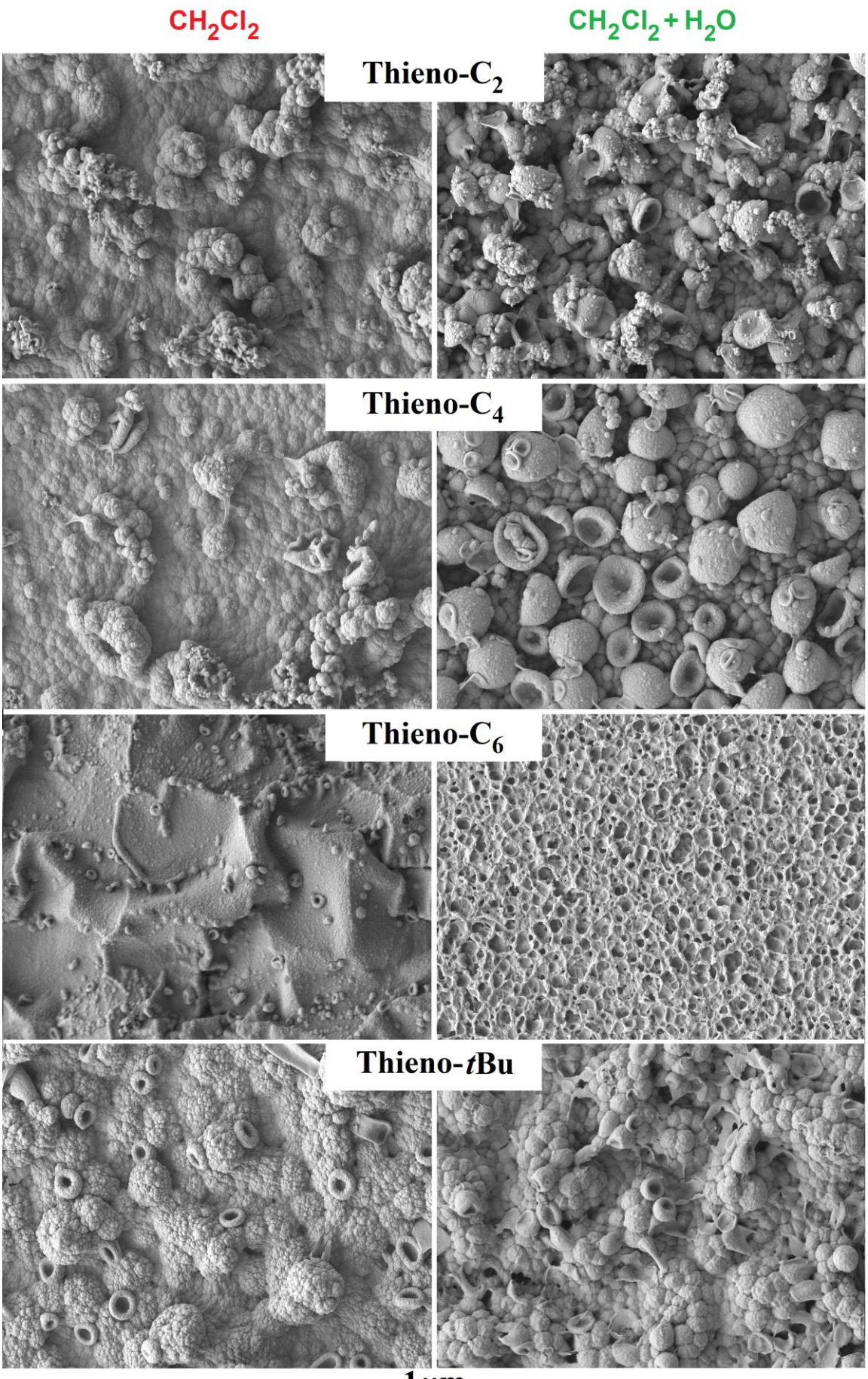
CH_2Cl_2
$CH_2Cl_2 + H_2O$
Thieno-C_2
Thieno-C_4
Thieno-C_6
Thieno-*t*Bu
1 μm

Figure 3. SEM images of polymer surfaces obtained from Thieno-C_2, Thieno-C_4, Thieno-C_6 and Thieno-*t*Bu via cyclic voltammetry (3 scans) and using CH_2Cl_2 (left hand column) or CH_2Cl_2 + H_2O (right column) as solvent.

With rigid substituents (perfluorinated and aromatic groups), both hollow spheres and/or nanotubular structures of different size are observed from polymerization in CH_2Cl_2 + H_2O (Figure 4 and Figure 5). Particularly, a higher number of porous structures is obtained from polymerization of Thieno-Ph. The influence of the linker is also very significant [46] as shown in Table 1. As an example, Figure 6 displays surfaces formed from two monomers bearing a pyrene substituent but having different linkers (carbamate and ester). Here, the number of porous structures is much higher with the ester linker compared to the carbamate one.

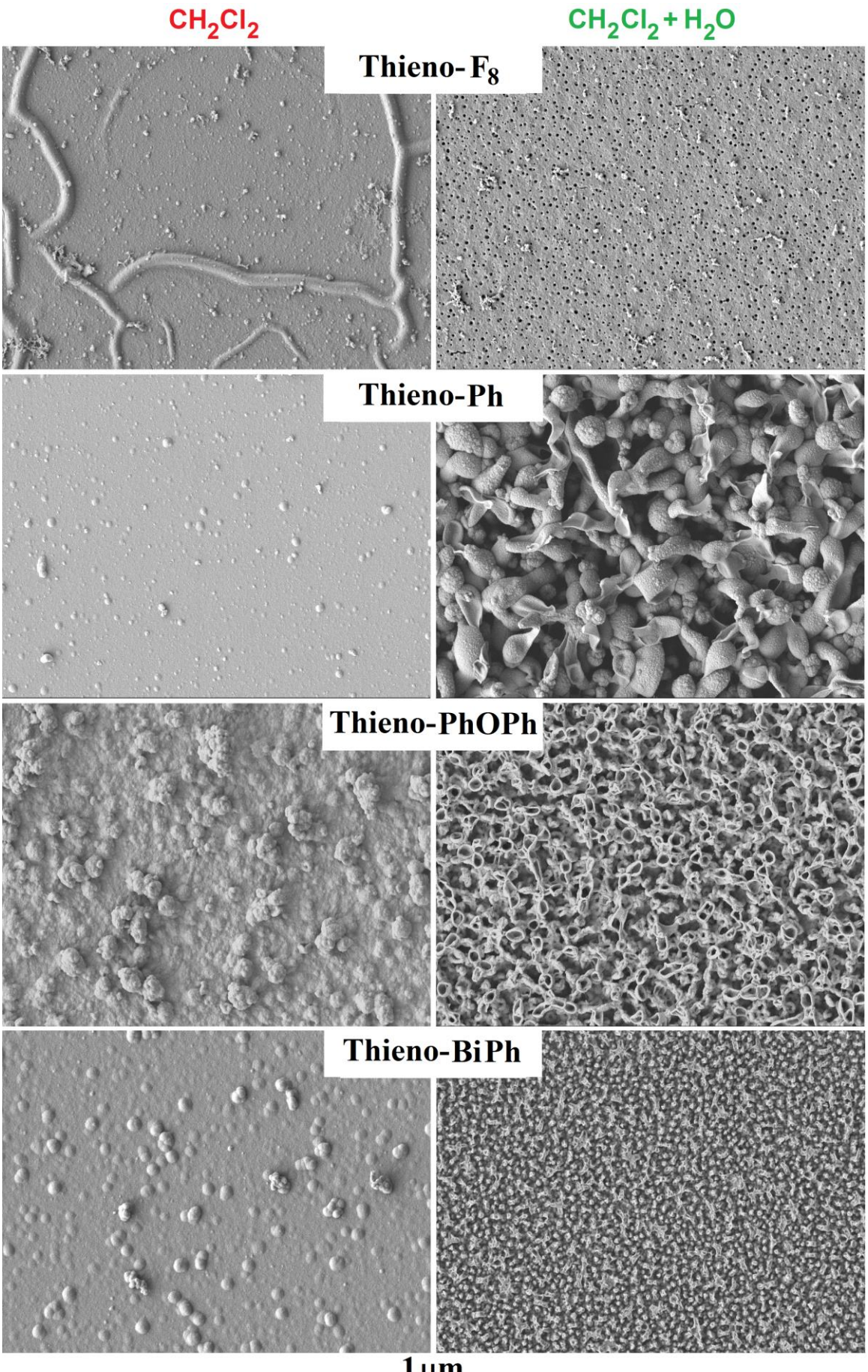
CH_2Cl_2
$CH_2Cl_2 + H_2O$
Thieno-F_8
Thieno-Ph
Thieno-PhOPh
Thieno-BiPh
1 μm

Figure 4. SEM images of polymer surfaces obtained from Thieno-F_8, Thieno-Ph, Thieno-PhOPh and Thieno-BiPh via cyclic voltammetry (3 scans) and using CH_2Cl_2 (left hand column) or CH_2Cl_2 + H_2O (right column) as solvent.

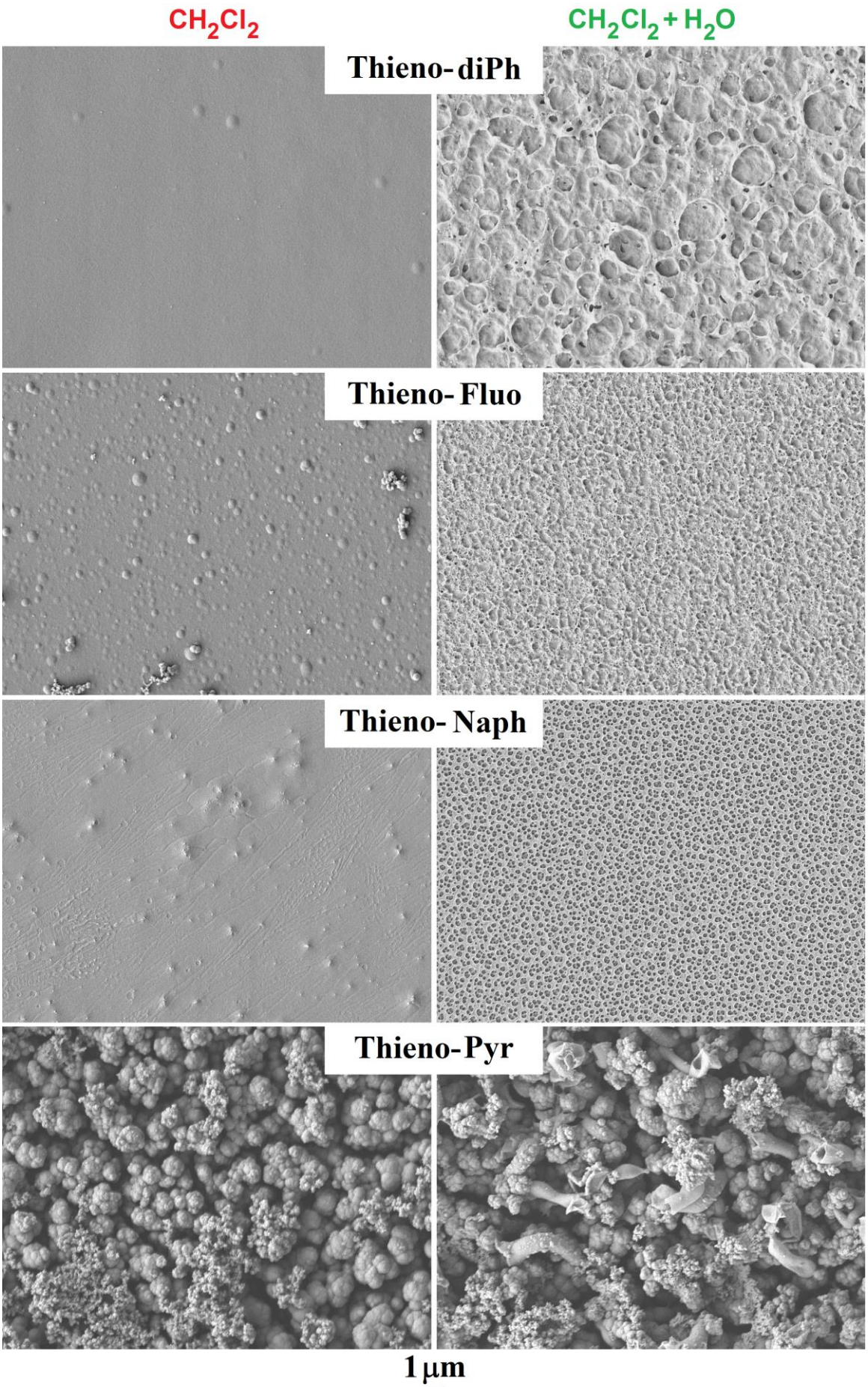
CH_2Cl_2
$CH_2Cl_2 + H_2O$
Thieno-diPh
Thieno-Fluo
Thieno-Naph
Thieno-Pyr
1 µm

Figure 5. SEM images of polymer surfaces obtained from Thieno-F_8, Thieno-Ph, Thieno-PhOPh and Thieno-BiPh via cyclic voltammetry (3 scans) and using CH_2Cl_2 (left hand column) or CH_2Cl_2 + H_2O (right column) as solvent.

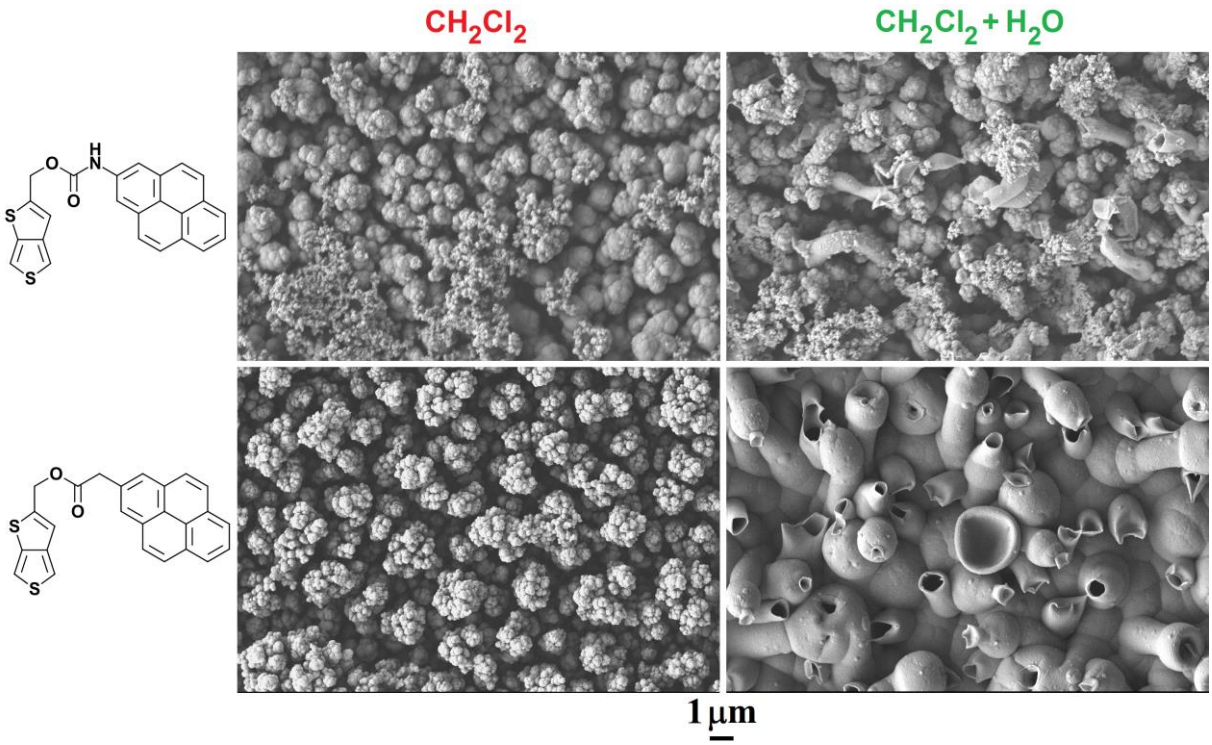

Figure 6. SEM images of polymer surfaces obtained from two different monomers differing by the linker via cyclic voltammetry (3 scans) and using CH_2Cl_2 (left hand column) or CH_2Cl_2 + H_2O (right column) as solvent.

Table 1. Example of surface morphology obtained with different linkers.

Monomer	Surface morphology	Monomer	Surface morphology
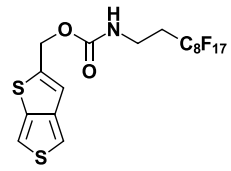	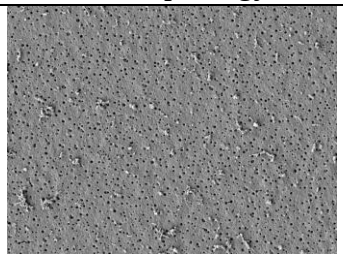	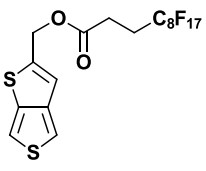	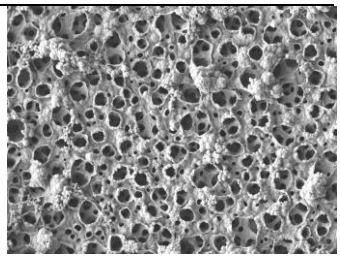
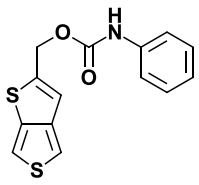	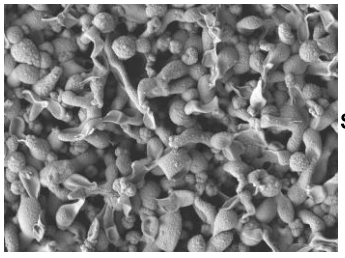	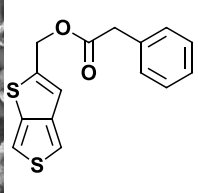	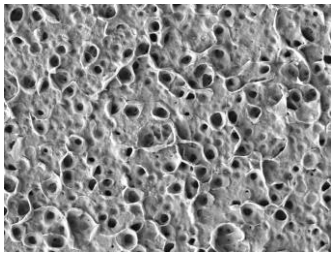

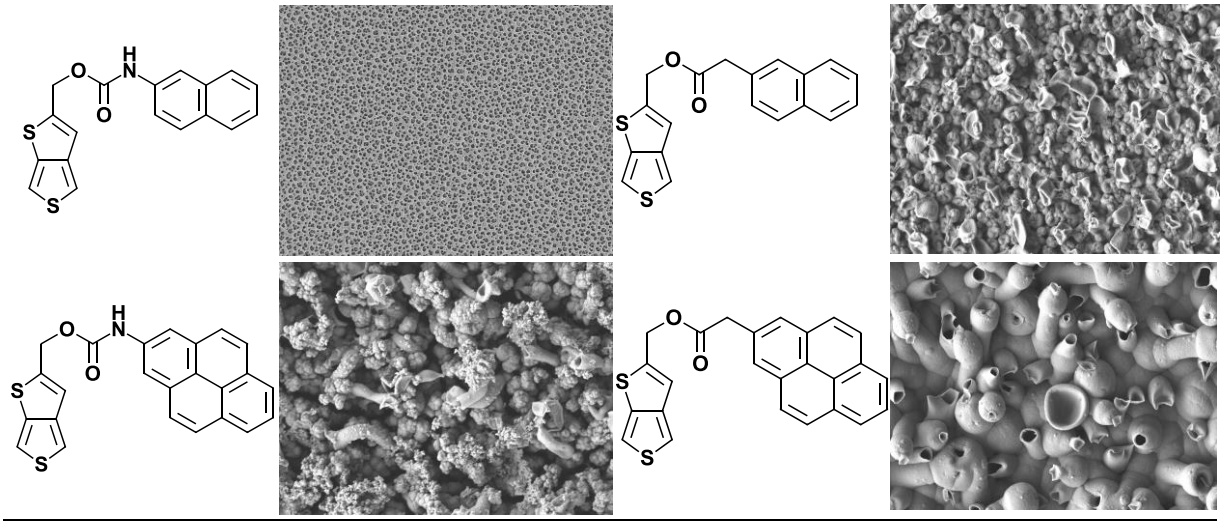

It is worth commenting on the formation of nanoporous membranes using Thieno-Naph (Figure 7). In this case, the pore size was found to be independent on the number of deposition scans. In order to better evaluate the influence of H_2O content on the formation of nanoporous membranes with Thieno-Naph, the solvent CH_2Cl_2 + H_2O was simply diluted by CH_2Cl_2. The percentages tested were 35% and 65% of CH_2Cl_2 + H_2O *vs* CH_2Cl_2. With these studies, we observe a large influence of H_2O content (Figure 8). At a low H_2O content (CH_2Cl_2 + H_2O (35%)), the formation of nanotubular structures is observed. When the H_2O content increases (CH_2Cl_2 + H_2O (65%)), a large increase in the number of nanotubular structures is observed. Here, the formation of nanoporous membranes is obtained especially with 100% of CH_2Cl_2 + H_2O.

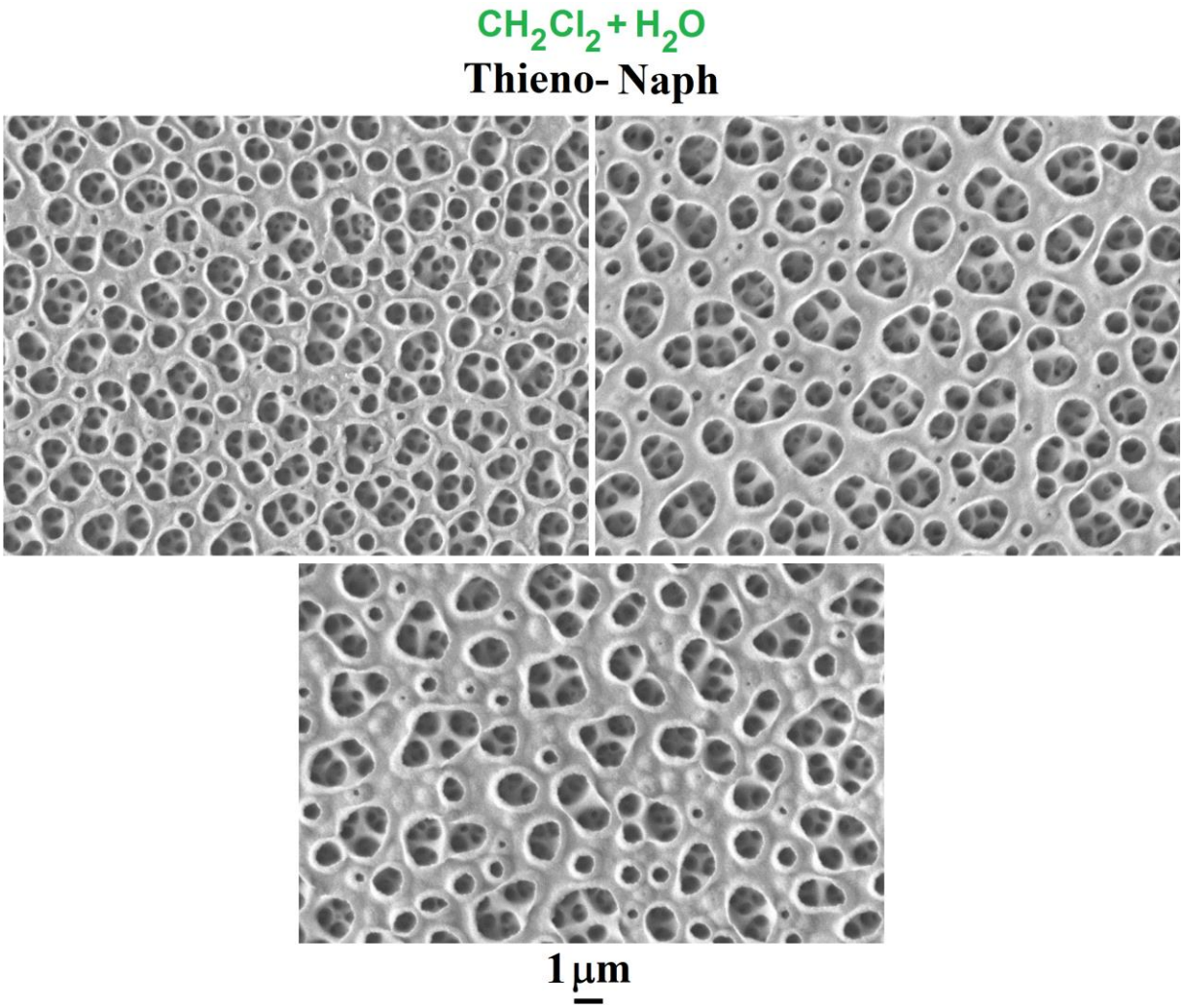

Figure 7. SEM images of polymer surfaces obtained from Thieno-diPh, Thieno-Fluo, Thieno-Naph and Thieno-Pyr via cyclic voltammetry (3 scans) and using CH_2Cl_2 (left hand column) or CH_2Cl_2 + H_2O (right column) as solvent.

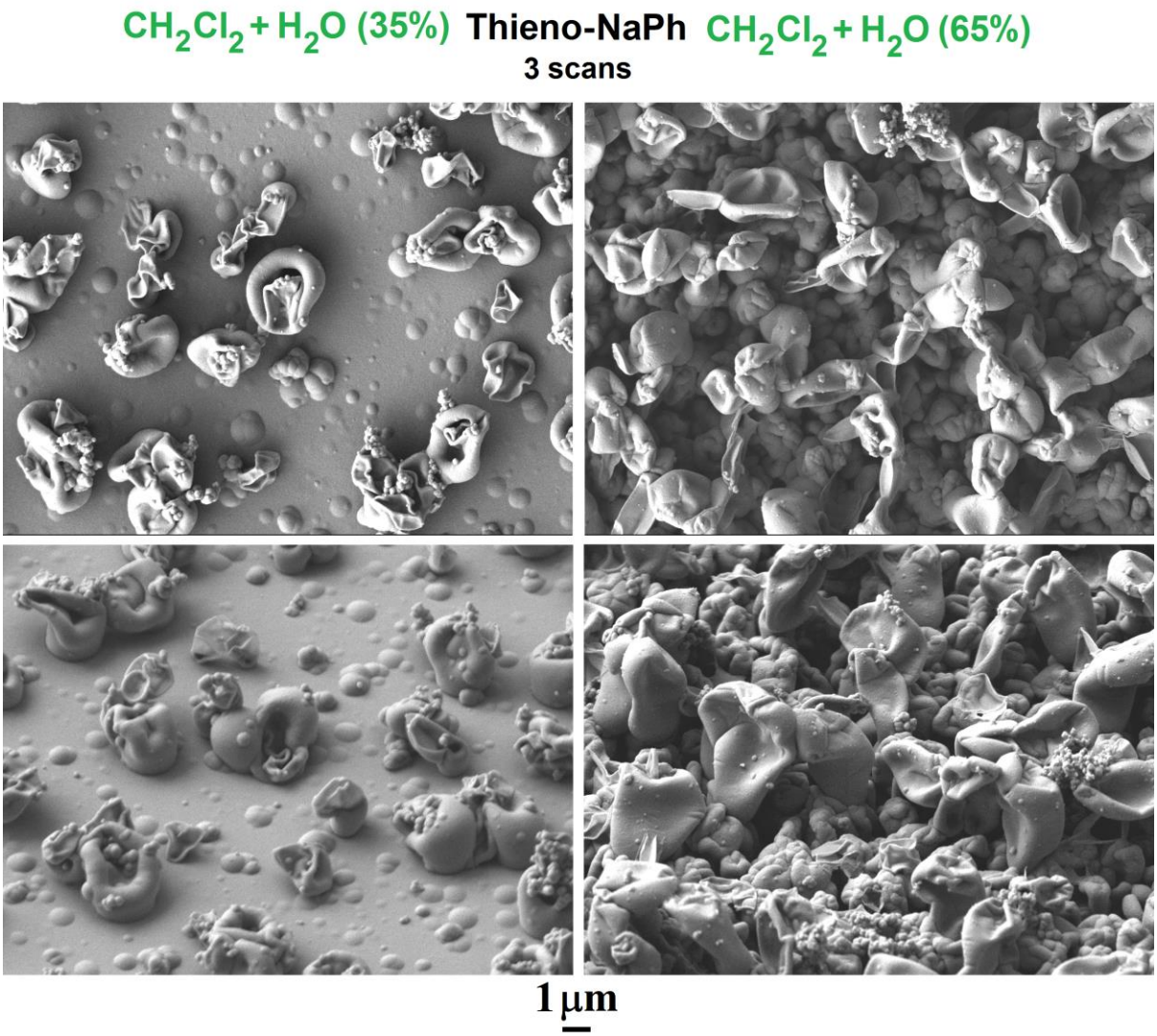

Figure 8. On the top, SEM images of polymer surfaces obtained from electrodeposition of Thieno-NaPh in CH_2Cl_2 + H_2O (35%) and CH_2Cl_2 + H_2O (65%) via cyclic voltammetry after 3 scans. On the bottom, the same surfaces but with an inclination angle of 45°.

Surface hydrophobicity of all surfaces after electrodeposition was characterized by measuring water contact angles (Table 2 and Table 3). The most hydrophobic surfaces were obtained from the monomers bearing the shortest hydrocarbon chains (e.g. Thieno-C_2) since these surfaces are very rough and the large number of hollow spheres present on the interface cause an increase in θ_w to 150.9°. With monomers bearing aromatic substituents, extremely high θ_w are also measured with Thieno-Ph, Thieno-PhOPh, Thieno-BiPh and Thieno-Pyr. The water adhesion on these surfaces is also extremely strong. Water droplets placed on these surfaces remain stuck even when the surface is inclined to 90°. An example of this behavior is given in Figure 9.

Table 2. Wettability data for the polymer films obtained by cyclic voltammetry in CH_2Cl_2.

Polymer	Number of deposition scans	θ_w [deg]
PolyThieno-C_2	1	78.3 ± 1.2
	3	67.7 ± 5.4
	5	130.6 ± 7.0
PolyThieno-C_4	1	38.6± 1.2
	3	96.8 ± 3.1
	5	114.8 ± 5.1
PolyThieno-C_6	1	96.3 ± 2.9
	3	91.3 ± 7.1
	5	105.1 ± 6.1
PolyThieno-tBu	1	86.2 ± 4.4
	3	95.3 ± 4.9
	5	103.4 ± 5.5
PolyThieno-F_8	1	102.3 ± 1.5
	3	111.6 ± 2.7
	5	122.5 ± 2.6
PolyThieno-Ph	1	76.2 ± 3.3
	3	88.8 ± 3.4
	5	95.9 ± 2.5
PolyThieno-PhOPh	1	90.7 ± 1.8
	3	109.4 ± 1.9
	5	113.7 ± 2.6
PolyThieno-Biph	1	112.0 ± 2.1
	3	91.9 ± 1.7
	5	114.7 ± 2.1
PolyThieno-diPh	1	80.5 ± 4.3
	3	97.6 ± 1.4
	5	95.3 ± 2.8
PolyThieno-Fluo	1	75.3 ± 2.8
	3	84.1 ± 1.4
	5	104.5 ± 3.2
PolyThieno-Naph	1	72.7 ± 4.4
	3	74.0 ± 4.1
	5	81.9 ± 2.3
PolyThieno-Pyr	1	126.4 ± 1.0
	3	128.1 ± 1.4
	5	130.3 ± 4.2

Table 3. Wettability data for the polymer films obtained by cyclic voltammetry in CH_2Cl_2 + H_2O.

Polymer	Number of deposition scans	θ_w [deg]
PolyThieno-C_2	1	46.8 ± 2.9
	3	86.4 ± 5.0
	5	150.9 ± 5.1
PolyThieno-C_4	1	47.9 ± 5.9
	3	83.8 ± 7.6
	5	98.9 ± 7.4
PolyThieno-C_6	1	65.4 ± 3.1
	3	72.2 ± 11.0
	5	84.2 ± 7.9
PolyThieno-tBu	1	61.2 ± 6.1
	3	60.5 ± 2.1
	5	97.4 ± 6.9
PolyThieno-F_8	1	126.8 ± 1.7
	3	119.1 ± 0.9
	5	131.7 ± 5.1
PolyThieno-Ph	1	71.3 ± 3.2
	3	121.8 ± 8.2
	5	107.2 ± 8.8
PolyThieno-PhOPh	1	106.0 ± 2.2
	3	107.5 ± 5.6
	5	125.5 ± 4.0
PolyThieno-Biph	1	113.3 ± 1.5
	3	122.9 ± 2.3
	5	131.8 ± 5.1
PolyThieno-diPh	1	81.1 ± 6.8
	3	75.2 ± 4.6
	5	104.4 ± 2.6
PolyThieno-Fluo	1	75.0 ± 4.9
	3	86.6 ± 2.2
	5	80.5 ± 3.9
PolyThieno-Naph	1	91.3 ± 1.4
	3	92.2 ± 2.4
	5	91.9 ± 6.1
PolyThieno-Pyr	1	86.8 ± 5.4
	3	140.9 ± 3.2
	5	131.5 ± 4.4

Figure 9. Picture of a water droplet on polymer surfaces obtained from Thieno-Pyr via cyclic voltammetry (3 scans) and using CH_2Cl_2 + H_2O as solvent. The substrate is inclined at 60°.

3.2.2. Surface chemistry

Moreover, the films were also chemically characterized. Examples of infrared (IR) spectra recorded by ATR are given in Figure 10. The IR spectra are relatively close. A peak is present at ≈ 3100-3200 cm^{-1} for N-H stretching as well as two peaks at ≈ 1735 and 1700 cm^{-1} for C=O(O) and C=O(NH) stretching and one peak at ≈ 1610 cm^{-1} for N-H bending. Another peak at ≈ 1000 cm^{-1} for C-O stretching is also present.

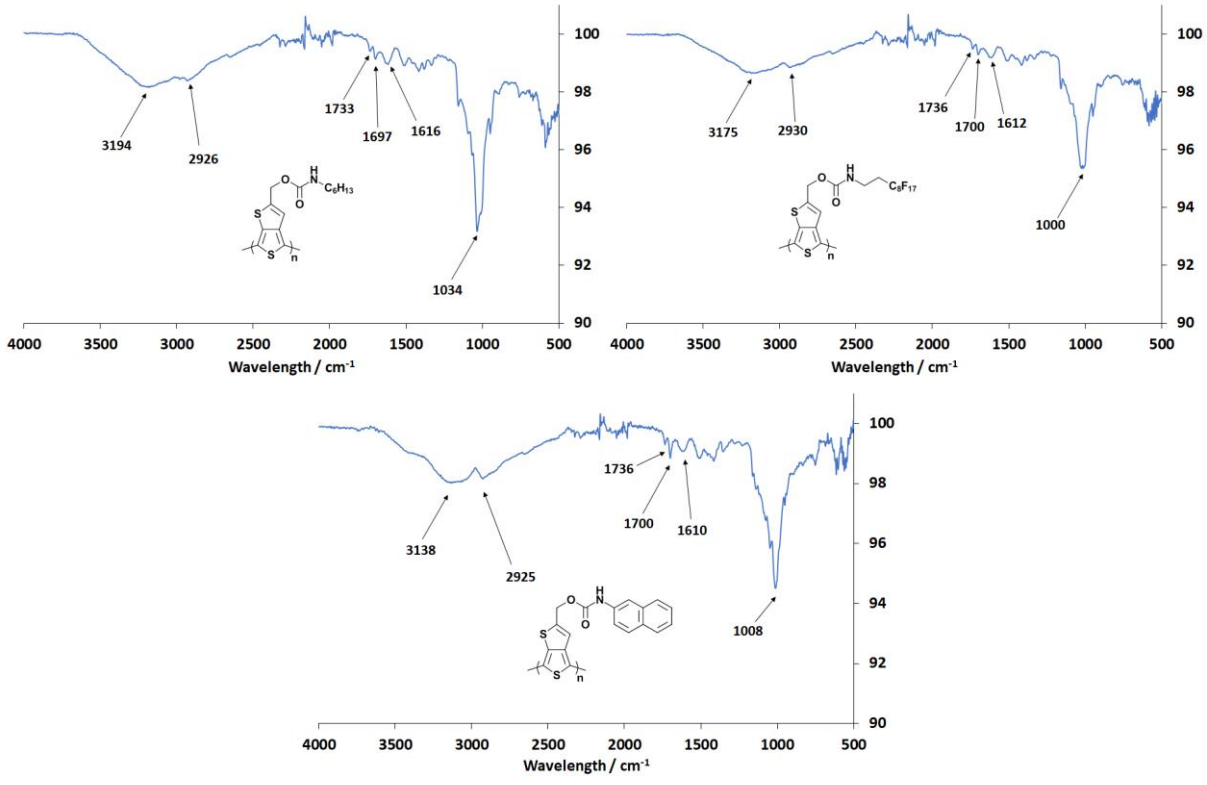

Figure 10. Infrared spectra of polymer surfaces obtained from Thieno-C_6, Thieno-F_8 and Thieno-Naph via cyclic voltammetry (3 scans) and using CH_2Cl_2 as solvent.

The films were also chemically characterized by EDX. An intense peak of the gold confirms the presence of gold on the substrate. For the polymers, peaks characteristic of the presence of C, N, O and S are clearly present in the spectra. The intensity of peak is different because the polymer thickness is not the same. The main difference observed is a peak characteristic of the presence of F in the polymer films obtained with Thieno-F_8.

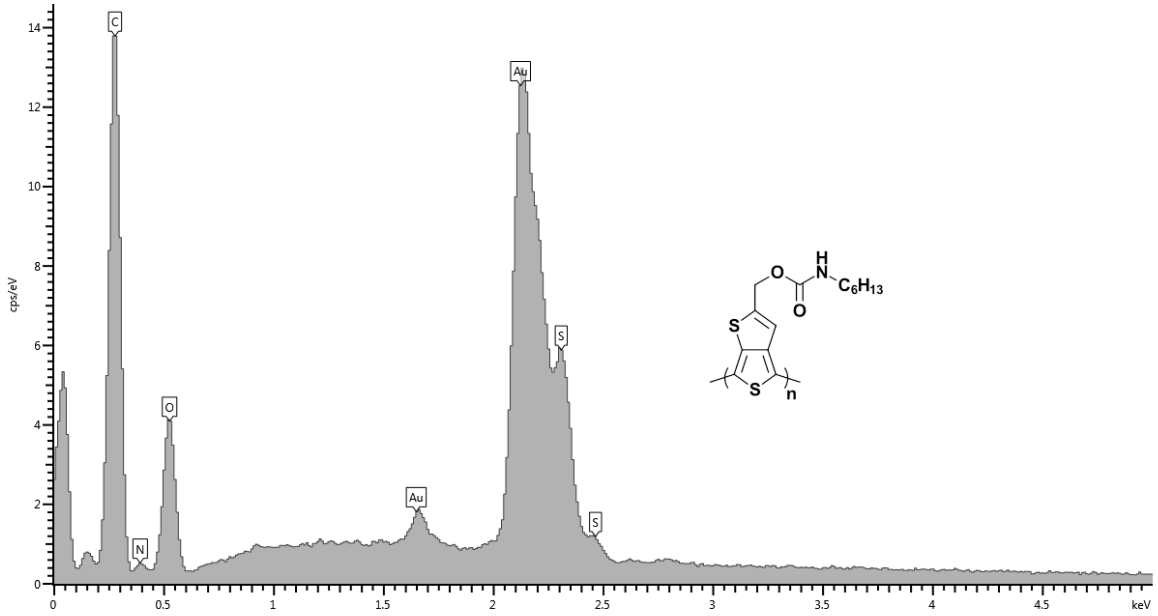
cps/eV
C
Au
O
N
S
keV
H
N
O
C_6H_{13}
n

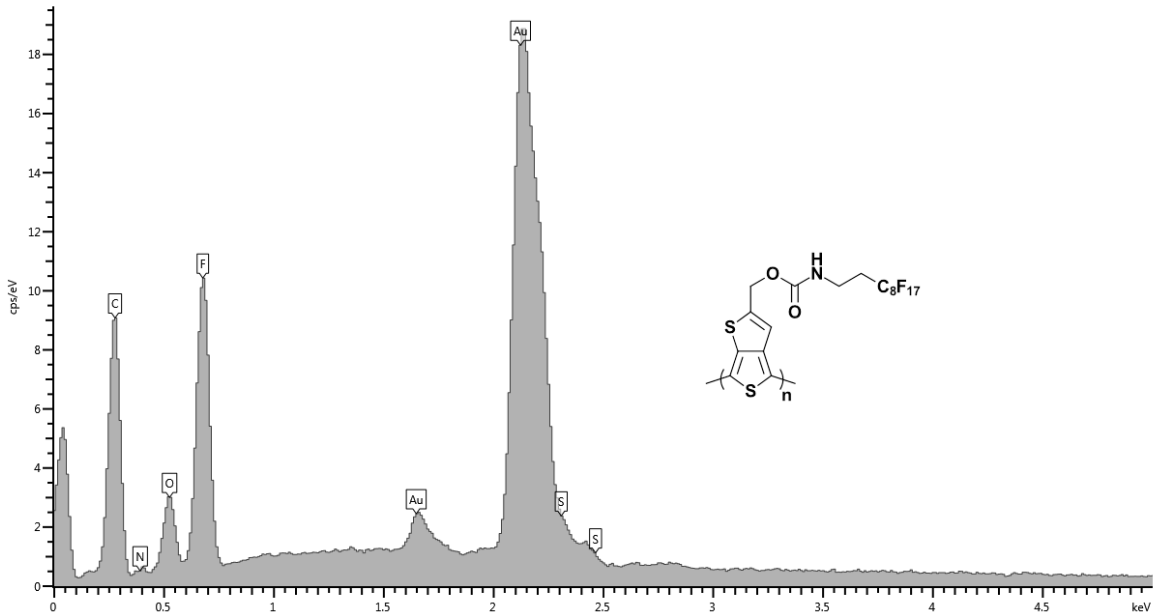
cps/eV
F
C
Au
O
N
S
keV
H
N
O
C_8F_{17}
n

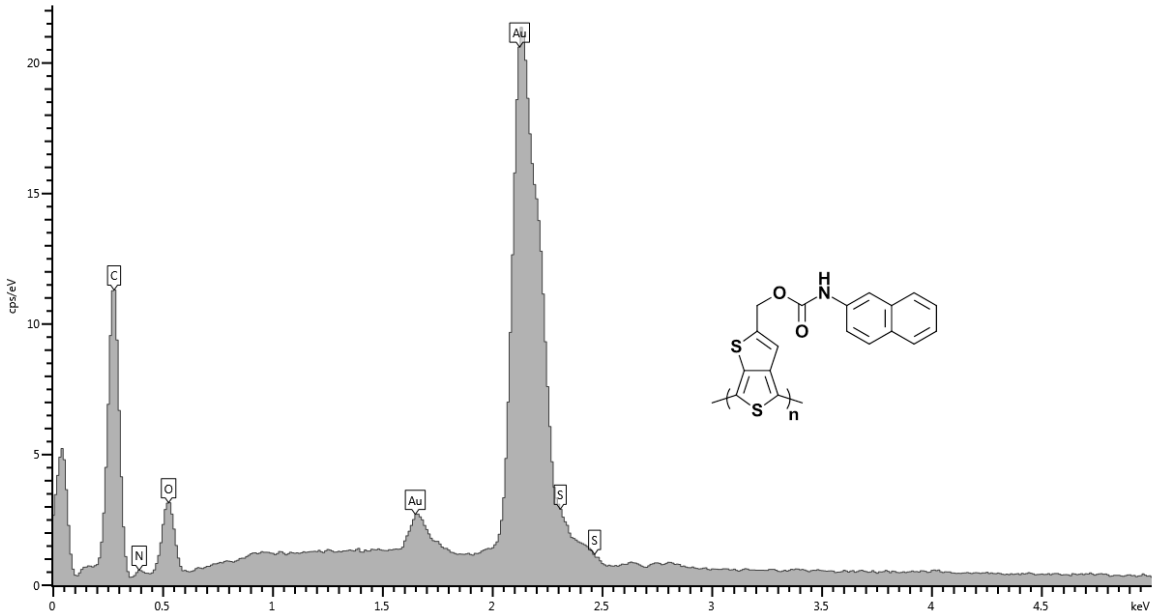
cps/eV
C
Au
O
N
S
keV
H
N
O
n

Figure 11. EDX spectra of polymer surfaces obtained from Thieno-C_6, Thieno-F_8 and Thieno-Naph via cyclic voltammetry (3 scans) and using CH_2Cl_2 as solvent.

Conclusion

In this work, we demonstrated the ability to obtain nanoporous structures using a templateless electropolymerization method in organic solvent (CH_2Cl_2) and without the aid of surfactant. Using thieno[3,4-*b*]thiophene monomers with polar carbamate linkers and various substituents, different porous structures were obtained especially when a significant fraction of water was included in the electrodeposition solvent (e.g., CH_2Cl_2 + H_2O). For example, hollow spheres or nanorings were observed with thieno[3,4-*b*]thiophene monomers bearing alkyl chains and nanotubular structures are observed from monomers bearing aromatic side groups. For the majority of surfaces developed, an increase in the surface hydrophobicity and water adhesion was observed. Many applications could be envisaged for these surfaces in separation water harvesting systems, membranes, opto-electronic devices or sensors.

References

[1] Y. Cheng, H. Yang, Y. Yang, J. Huang, K. Wu, Z. Chen, X. Wang, C. Lin, Y. Lai, J. Mater. Chem. B 6 (2018) 1862–1886.

[2] O.S. Kwon, S.J. Park, J.S. Lee, E. Park, T. Kim, H.-W. Park, S.A. You, H. Yoon, J. Jang, Nano Lett. 12 (2012) 2797–2802.

[3] C.J. Shearer, A. Cherevan, D. Eder, Adv. Mater. 26 (2014) 2295–2318.

[4] Y.-Z. Long, M.-M. Li, C. Gu, M. Wan, J.-L. Duvail, Z. Liu, Z. Fan, Prog. Polym. Sci. 36 (2011) 1415–1442.

[5] E. Khosravifard, M. Salavati-Niasari, M. Dadkhah, G. Sodeifian, J. Nanostruct. 2 (2012) 191–197.

[6] M. Mahdiani, F. Soofiv, F. Ansari, M. Salavati-Niasari, J. Clean. Prod. 176 (2018) 1185–1197.

[7] M. Mahdiani, A. Sobhani, M. Salavati-Niasari, Sep. Purif. Technol. 185 (2017) 140–148.

[8] A. Salehabadi, M. Salavati-Niasari, M. Ghiyasiyan-Arani, J. Alloy. Compd. 745, 2018, 789–797.

[9] M. Salavati-Niasari, M. Bazarganipour, Appl. Surf. Sci. 255 (2008) 2963–2970.
[10] M. Salavati-Niasari, F. Davar, M. Bazarganipour, Dalton Trans. 39 (2010) 7330–7337.
[11] M. Salavati-Niasari, M. Bazarganipour, Appl. Surf. Sci. 255 (2009) 7610–7617.
[12] M. Salavati-Niasari, M. Bazarganipour, J. Mol. Catal. A-Chem. 278 (2007), 173–180.
[13] M. Salavati-Niasari, E. Esmaeili, H. Seyghalkar, M. Bazarganipour, Inorg. Chim. Acta 375 (2011) 11–19.
[14] M. Salavati-Niasari, A. Badiei, K. Saberyan, Chem. Eng. J. 173 (2011) 651–658.
[15] A. Amiri, M. Shanbedi, M. Savari, B. T. Chew, S. N. Kazi, RSC Adv. 5 (2015) 71144–71152.
[16] L. Qu, L. Dai, M. Stone, Z. Xia, Z.L. Wang, Science 322 (2008) 238–242.
[17] L. Ge, S. Sethi, L. Ci, P.M. Ajayan, A. Dhinojwala, Proc. Natl. Acad. Sci. U. S. A. 104 (2007) 10792–10795.
[18] S. Ozden, L. Ge, T.N. Narayanan, A.H.C. Hart, H. Yang, S. Sridhar, R. Vajtai, P.M. Ajayan, ACS Appl. Mater. Interfaces 6 (2014) 10608–10613.
[19] L. Qu, L. Dai, Adv. Mater. 19 (2007) 3844–3849.
[20] Z. Cheng, J. Gao, L. Jiang, Langmuir 26 (2010) 8233–8238.
[21] J. Fu, F. Yang, Z. Guo, Mater. Lett. 236 (2019) 732–735.
[22] Z. Wang, Y. Wang, G. Liu, Angew. Chem. Int. Ed. 55 (2016) 1291–1294.
[23] Z. Sun, T. Liao, W. Li, Y. Dou, K. Liu, L. Jiang, S.-W. Kim, J.H. Kim, S.X. Dou, NPG Asia Mater. 7 (2015) e232.
[24] M. Paulose, H.E. Prakasam, O.K. Varghese, L. Peng, K.C. Popat, G.K. Mor, T.A. Desai, C.A. Grimes, J. Phys. Chem. C 111 (2007) 14992–14997.
[25] L. Lee, S.J. Park, Chem. Rev. 114 (2014) 7487–7556.
[26] J. Yu, S. Xiang, M. Ge, Z. Zhang, J. Huang, Y. Tang, L. Sun, C. Lin, Y. Lai, Coatings 8 (2018) 374.
[27] H.-A. Lin, S.-C. Luo, B. Zhu, C. Chen, Y. Yamashita, H.-h. Yu, Adv. Funct. Mater. 23 (2013) 3212–3219.
[28] R. Xiao, S.I. Cho, R. Liu, S.B. Lee, J. Am. Chem. Soc. 129 (2007) 4483–4489.
[29] L. Qu, G. Shi, J. Yuan, G. Han, F. Chen, J. Electroanal. Chem. 561 (2004) 149−156.
[30] C. Debiemme-Chouvy, Electrochem. Solid-State Lett. 10 (2007) E24−E26.
[31] A. Fakhry, H. Cachet, C. Debiemme-Chouvy, Electrochim. Acta 179 (2015) 297−303.
[32] A. Fakhry, F. Pillier, C. Debiemme-Chouvy, J. Mater. Chem. A 2 (2014) 9859−9865.
[33] C. Debiemme-Chouvy, Biosens. Bioelectron. 25 (2010) 2454−2457.
[34] C. Debiemme-Chouvy, Electrochem. Commun. 11 (2009) 298-301.

[35] L. Qu, G. Shi, F. Chen, J. Zhang, Macromolecules 36 (2003) 1063−1067.
[36] J. Yuan, L. Qu, D. Zhang, G. Shi, Chem. Commun. 0 (2004) 994−995.
[37] C. Debiemme-Chouvy, A. Fakhry, F. Pillier, Electrochim. Acta 268 (2018) 66–72.
[38] J. T. Kim, S. K. Seol, J. H. Je, Y. Hwu, G. Margaritondo, Appl. Phys. Lett. 94 (2009) 034103.
[39] B. Parakhonskiy, D. Shchukin, Langmuir 31 (2015) 9214−9218.
[40] T. Darmanin, F. Guittard, J. Mater. Chem. A 4 (2016) 3197–3203.
[41] C.R. Szczepanski, I. M'Jid, T. Darmanin, G. Godeau, F. Guittard, J. Mater. Chem. A 4 (2016) 17308–17323.
[42] S. Bai, Q. Hu, Q. Zeng, M. Wang, L. Wang, ACS Appl. Mater. Interfaces 10 (2018) 11319–11327.
[43] G. Ramos Chagas, F. Guittard, T. Darmanin, ACS Appl. Mater. Interfaces 8 (2016) 22732–22743.
[44] G. Ramos Chagas, T. Darmanin, G. Godeau, F. Guittard, Electrochim. Acta 269 (2018) 462–478.
[45] O. Thiam, A. Diouf, D. Diouf, S. Y. Dieng, F. Guittard, T. Darmanin, Phil. Trans. R. Soc. A 377 (2019) DOI: 10.1098/rsta.2019.0123.
[46] O. Sane, A. Diouf, M. Pan, G. Morán Cruz, F. Savina, R. Méallet-Renault, S. Y. Dieng, S. Amigoni, F. Guittard, T. Darmanin, Electrochim. Acta 320 (2019) 134594.
[47] O. Sane, A. Diouf, G. Morán Cruz, F. Savina, R. Méallet-Renault, S. Amigoni, S. Y. Dieng, F. Guittard, T. Darmanin, Mater. Today, DOI: 10.1016/j.mattod.2019.09.020.
[48] G. Ramos Chagas, G. Morán Cruz, R. Méallet-Renault, A. Gaucher, D. Prim, D.E. Weibel, S. Amigoni, F. Guittard, T. Darmanin, React. Funct. Polym. 135 (2019) 65–76.
[49] A. Patra, Y.H. Wijsboom, G. Leitus, Chem. Mater. 23 (2011) 896–906.
[50] G. Buemi, Bull. Chem. Soc. Jpn. 62 (1989) 1262–1268.
[51] Y. Wada, Y. Asada, T. Ikai, K. Maeda, T. Kuwabara, K. Takahashi, S. Kanoh, ChemistrySelect 1 (2016) 703–709.